JOM, Vol. 76, No. 6, 2024
https://doi.org/10.1007/s11837-024-06556-9

A Well-Posed Definition for Plastic Strain Rate in Indentation

D.S. STONE ,[1,5,] J.E. JAKES,[2] and A.A. ELMUSTAFA[3,4]

1.—Department of Materials Science and Engineering, University of Madison-Wisconsin, Madison, WI 53705, USA. 2.—Forest Biopolymers Science and Engineering, USDA Forest Service, Forest Products Laboratory, Madison, WI 53726, USA. 3.—Department of Mechanical and Aerospace Engineering, Old Dominion University, Norfolk, VA 23529, USA. 4.—The Applied Research Center-Thomas Jefferson National Accelerator Facility, Newport News, VA 23606, USA. 9.—e-mail: dsstone@wisc.edu

To compare hardness versus strain rate data from different kinds of indentation creep test can be challenging. It is often difficult to determine whether measured differences in material response along different loading paths, such as constant load creep or load relaxation, are real or merely arise as artifacts from the analysis. We argue that the difficulty lies in how indentation strain rate is defined. For traditional definitions of strain rate, such as $\dot{\varepsilon}_h$, which measures the rate of penetration, or $\dot{\varepsilon}_A$, which measures the growth of indent area, material response might seem path-dependent even when it is not. We introduce a new definition of plastic strain rate, $\dot{\varepsilon}_{irr}$, which is based on irreversible work and is well-posed in the sense that it gives the same results from different loading paths when deformation is path-independent. This property frees experimenters to isolate and explore deformation mechanisms that respond differently along different loading paths, which is useful for revealing the influences of time and strain rate on evolution of structure. $\dot{\varepsilon}_{irr}$ is important for exploring path-dependence in high-hardness/modulus ($\gtrsim 0.02$) materials like ceramics and polymers. For low-hardness-modulus materials other measures of strain rate suffice.

List of Symbols

α	Cone half-angle
A	Instantaneous projected area of the indent
β	E_{eff}/E_r
χ	Work-hardening exponent in constitutive model $= -M/N$
E_{eff}	"Effective" modulus of contact $= S/\sqrt{A}$
E_r	"Reduced" contact modulus: $= \left[\left(1-\nu_d^2\right)/E_d + \left(1-\nu_s^2\right)/E_s\right]^{-1}$
E_d, ν_d	Young's modulus and Poisson's ratio of diamond
E_s, ν_s	Young's modulus and Poisson's ratio of specimen
$\overline{\varepsilon}$	Von Mises effective plastic strain
ε_p	(True) plastic strain in uniaxial loading
$\dot{\overline{\varepsilon}}$	Von Mises effective plastic strain rate
$\dot{\varepsilon}$	(True) strain rate in uniaxial loading
$\dot{\varepsilon}_A$	Area-based strain rate $= (1/2)\left(\dot{A}/A\right)$
$\dot{\varepsilon}_{irr}$	Irreversible work-based strain rate
$\dot{\varepsilon}_h$	Depth-based strain rate $= \dot{h}/h$
$\dot{\varepsilon}_p$	Plastic strain rate under uniaxial loading
H	Instantaneous Meyer hardness
h	Instantaneous depth of indentation
h_e	Elastic depth $= h - h_f$
h_f	Final depth of indentation, Fig. 10
K	Coefficient for unloading in $P = Kh_e^n$
κ	Rate parameter in constitutive model
M, N	Power law exponents in constitutive model
m_σ	Strain rate sensitivity exponent for the flow stress
m_H	Strain rate sensitivity exponent for hardness
n	Power law exponent for unloading $P = Kh_e^n$
P	Instantaneous load
S	Contact stiffness
σ	(True) stress in uniaxial loading
$\overline{\sigma}$	Von Mises effective stress
V	Dummy variable representing volume in integration
ξ	Dummy variable representing depth in integration

(Received November 15, 2023; accepted March 26, 2024; published online May 10, 2024)

INTRODUCTION

The term "indentation creep" refers to a class of experiments for measuring rate-sensitive plasticity using a nanoindenter. Indentation creep can be used for measuring high-temperature creep exponents[1–4] and low-temperature activation volumes for plastic deformation.[5–9] Indentation creep can be extended beyond metals and ceramics to characterize a wide range of materials including polymers and biomaterials.[10–25] Indentation creep can also measure rate-sensitive plasticity across a wide dynamic range of strain rates, from 10^{-7}/s[7,26] to 10^{4}/s.[27]

By relying on complementary methods for measuring indentation creep, experimenters might be able to gain additional insight into deformation mechanisms, beyond what they can learn from measuring power law exponents and activation volumes alone. Specifically, if the deformation structures that develop during indentation are influenced by loading path—for instance, by how fast the indenter is initially driven into the specimen—then it might be possible to employ different loading paths to isolate time- and strain rate-dependent structural evolution along with the mechanisms that cause it. However, to explore the effects of loading path, it is important that we carefully specify a well-posed definition of strain rate so that, if a material is path-*independent*, then measurements of hardness versus strain rate along different loading paths give identical results. With this well-posed definition of strain rate, an experimenter can be confident that, if two experiments give different results, the differences arise from material behavior not the analysis.

In this article, we briefly review what we mean by path-independent and path-dependent deformation. We outline various types of indentation creep tests for measuring creep along different loading paths, and we review some different definitions of indentation strain rate. We then propose five criteria that a *well-posed* definition of strain rate must satisfy before it can serve as a valid basis for comparing measurements along different loading paths. We introduce a new definition of strain rate, $\dot{\varepsilon}_{\mathrm{irr}}$, that satisfies these criteria, and we demonstrate the utility of $\dot{\varepsilon}_{\mathrm{irr}}$ by using it to analyze some of our previously published data, both simulation and experiment.

Path-Independent and Path-Dependent Deformation

In plasticity theory, the concepts of path independence and path dependence are centered on the concept of a mechanical equation of state,[28,29] which helps to motivate our analysis. A simple form of path-independence is when, in plastic deformation, the uniaxial flow stress, σ, can be expressed in terms of plastic strain, ε_{p}, and strain rate, $\dot{\varepsilon}_{\mathrm{p}}$, through a state equation under monotonic loading:

$$\sigma = \sigma\left(\varepsilon_{\mathrm{p}}, \dot{\varepsilon}_{\mathrm{p}}\right) \tag{1}$$

A necessary condition for the equation of state is that the derivatives, obtained experimentally, commute: $\partial^2\sigma/\partial\varepsilon_{\mathrm{p}}\partial\dot{\varepsilon}_{\mathrm{p}} = \partial^2\sigma/\partial\dot{\varepsilon}_{\mathrm{p}}\partial\varepsilon_{\mathrm{p}}$.[29] Molybdenum is an example of a material for which plastic deformation can be well-described using a state equation, at least under a limited set of conditions. For molybdenum at low temperatures, under uniaxial loading and for strains that are not too large, both second derivatives are zero, so path-dependence is satisfied in a trivial way. In molybdenum, the flow stress is the sum of two components, one depending on work hardening and grain size but not strain rate and the other depending on strain rate but not work hardening or grain size. Work hardening—the accumulation of dislocations—is independent of strain rate at low temperatures because, apparently, thermal activation plays little or no role in the creation and annihilation of dislocations at low temperatures. Likewise, in molybdenum, the derivative of the flow stress with respect to strain rate reflects the role of thermal activation in overcoming the (high) Peierls barrier during dislocation glide, which is a property of the dislocation line but not dislocation density (work hardening).[30–32]

We have previously shown that, in molybdenum, the derivative of the hardness with respect to indentation strain rate is independent of work hardening[5] and grain size.[6] To within experimental error, hardness versus strain rate is independent of how it is measured: constant load creep, load relaxation, or rate-change experiments all give the same results. The data are also independent of how rapidly the indenter is loaded into the material.[21] We attribute these behaviors to the path-independence of the flow stress in molybdenum.

In most situations plastic deformation is path-*dependent*. An example is aluminum at room temperature, for which derivatives of flow stress with respect to strain and strain rate do not commute.[29] Early nanoindentation measurements on aluminum did not reveal any path dependence in hardness versus strain rate,[33] but experimental methods have improved, and it might now be possible to detect differences in aluminum based on loading path. Lucas and Oliver[34] explored path dependence in indentation creep of indium between 28°C and 75°C. They reported that hardness–strain rate measurements were strongly dependent on loading path (constant strain rate loading versus constant load creep; Fig. 1), which makes sense because time and strain rate effects strongly influence evolution of structure in metals at high homologous temperatures.

Tests for Measuring Indentation Creep

The typical nanoindentation experiment consists of a loading segment, a hold segment, and an unloading segment. Creep properties—by which we mean rate-sensitive plastic flow—can be

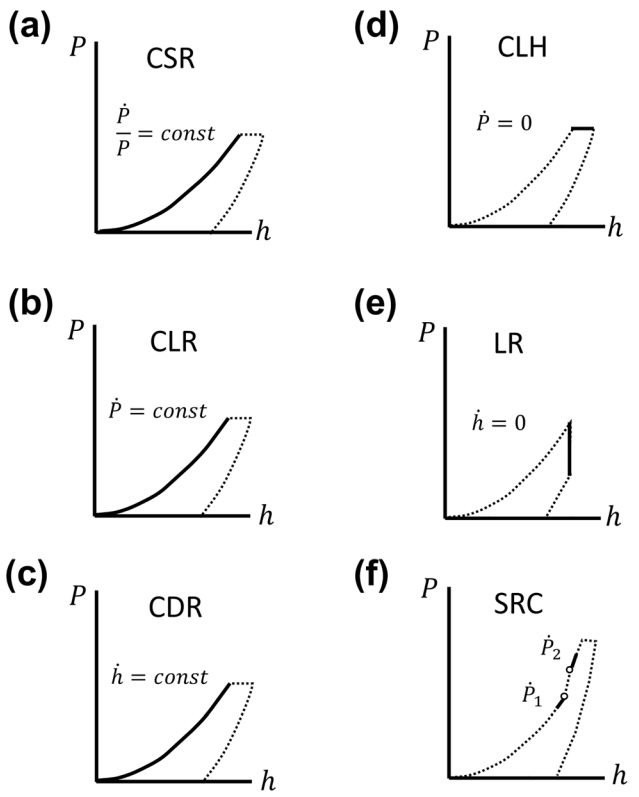

Fig. 1. Schematic load–depth (*P-h*) traces for some different protocols to measure indentation creep. The solid lines represent the portions of the tests analyzed for creep: (a) constant strain rate loading (*CSR*); (b) constant loading rate (*CLR*); (c) constant displacement rate (*CDR*); (d) constant load hold (*CLH*); e) load relaxation (*LR*); and f) rate-change experiment (*SRC*). Two or more protocols can be combined for a single indent.

measured during loading or hold. Figure 1 illustrates some different experimental protocols. The experiment might control instantaneous load (P) or depth (h), and both are recorded continuously during the experiment as functions of time (t). The constant strain rate experiment (CSR) is conducted such that $\dot{P}/P = \text{const}$ during loading,[34] where the dot above P signifies a time derivative. The constant loading rate (CLR) corresponds to $\dot{P} = \text{const}$, and and constant displacement rate (CDR) is $\dot{h} = \text{const}$ during loading. Other experimental protocols include constant load creep experiment (constant load hold; CLH; $\dot{P} = 0$)[4,35] and load relaxation (LR; $\dot{h} = 0$[36]). Finally, in a strain rate-change (SRC) experiment, one of the experimental controls, say $\dot{h}$[5] or $\dot{P}/P$,[37] is changed rapidly during loading so that the hardness at two different strain rates is measured at a fixed contact area. When comparing data from two protocols, it is helpful to generate the data from a single indent to reduce experimental uncertainty. For instance, CLR data can be generated from the loading portion of an indent that also measures constant load creep.

All these experiments probe deformation along different paths. For instance, for a pyramid- or cone-shaped indenter, the CSR test should be at constant structure, independent of the size of the indent (excluding an indentation size effect) because the deformation conditions are scale-independent; while in the constant load creep test the structure should change if structural evolution depends on strain rate. The most direct basis for comparing different loading paths is Meyer hardness versus strain rate. Meyer hardness, whose physical significance has been long established,[2,38] is defined as:

$$H = \frac{P}{A} \tag{2}$$

where P is the instantaneous load and A the instantaneous projected contact area. Until now, however, strain rate in an indentation test is not as well understood, nor is there a universal definition. The most commonly used definition of indentation strain rate is based on the rate of penetration as:

$$\dot{\varepsilon}_h = \frac{\dot{h}}{h} \tag{3}$$

This definition has obvious limitations in the analysis of indentation load relaxation where $\dot{h} = 0$ even though P and A change with time due to rate-sensitive deformation. Lucas and Oliver[34] proposed a strain rate definition of $(1/2)\left[\dot{P}/P - \dot{H}/H\right]$, which, by virtue of Eq. 2, is equivalent to $(1/2)\dot{A}/A$. We denote the area-based strain rate as:

$$\dot{\varepsilon}_A = \frac{1}{2}\frac{\dot{A}}{A} \tag{4}$$

Other definitions of strain rate include the Stone and Yoder plastic strain rate[5] which subtracts out elastic depth based on the Doerner–Nix approach,[39] and Phani et al.'s correction,[35] which appears similar to our $\dot{\varepsilon}_{irr}$, introduced below, but which is based on removing elastic displacements rather than subtraction out reversible work, which is our method.

A Well-Posed Definition of the Strain Rate

Path-dependent behavior is apparent in amorphous polymers below the glass transition.[21] Figures 2 and 3 show a typical example taken from polystyrene in an earlier paper.[21] Path dependence is revealed by the fact that the CLR and constant load creep data fall on separate traces, and constant load creep data with different initial strain rates also differ from each other. The experimental details are published in Ref. 21, but we outline some of the most salient points here. Separate indents were performed with a Berkovitch probe, to 10-mN maximum load, but with different loading times, ranging from 0.01 s to 100 s. The hardness and strain rates data of Figs. 2 and 3 are determined based on load–depth–time traces, which are calibrated against measured areas taken from

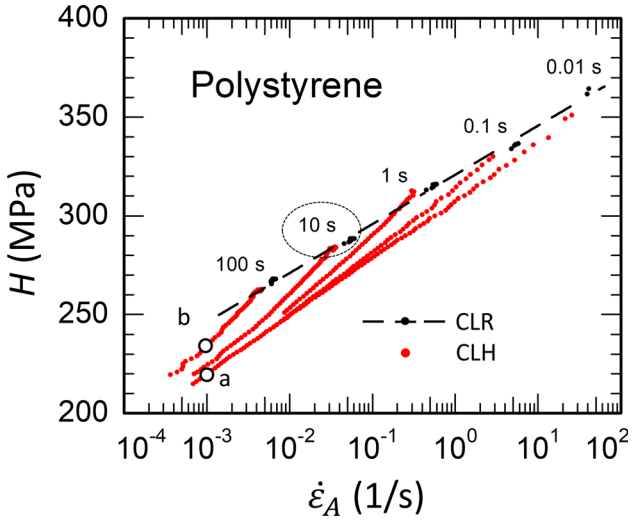

Fig. 2. Indentation creep of polystyrene from[11] based on $\dot{\varepsilon}_A$, suggesting path-dependent behavior based on constant loading rate (*CLR*) and constant load hold (*CLH*). A close-up of the circled 10-s loading data is given in Fig. 3.

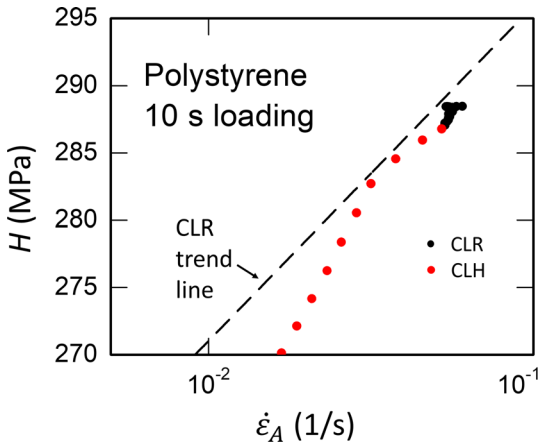

Fig. 3. Close-up of the data with an initial loading time of 10 s in Fig. 2.

interrupted creep.[21] We showed that, because the area in these experiments only changes due to plastic deformation, not viscoelastic deformation (viscoelasticity becomes important at low strain rates), the reported hardness values reflect yielding and not viscoelastic flow.[21,40] Each indent generates CLR data over a narrow range of strain rate at loads near the maximum, along with a continuous spectrum of constant load creep data extending across 3–5 decades of strain rate, depending on the initial loading rate. Collectively, the CLR data taken from different indents comprise a single set of data spanning 4 decades in strain rate. The CLR data in Fig. 2 agree to within about 5% with published data of compression yield versus strain rate, taking into account the ratio of hardness to flow stress at 8% strain.[21] Thus, the CLR data are a good proxy for yield strength versus strain rate. On the other hand, constant load creep data reveal that prior deformation at high strain rates causes softening at moderate and low strain rates. Points "a" and "b" in Fig. 2 show this effect for indents initially loaded in 0.01 s ($\dot{\varepsilon}_A = 50/s$) and 10 s ($\dot{\varepsilon}_A = 0.05/s$), respectively. Apparently, the material at point "a" is softer than the material at point "b" because the former was initially deformed at a higher rate. Again, the reduction in hardness is not an artifact of our analysis: we measured the areas of the indents, and they are different. In addition, all the different hardness–strain rate curves in Fig. 2 contain what appear to be transients in strain rate at the intersections between the CLR and constant load creep data. One such transient is shown in Fig. 3 where the 10-s loading data (circled region in Fig. 2) have been expanded. The dashed lines in Figs. 2 and 3 are a straight line least squares fit to the entire collection of CLR data at different strain rates. CLR data from the 10-s loading experiment fall slightly below the dashed line because of random error.

One might reasonably ask which features of the data in Figs. 2 and 3 are caused by material behavior, and which are caused by the way we analyze the data relying on H and $\dot{\varepsilon}_A$. To answer this question, we need to examine whether $\dot{\varepsilon}_A$ is *well-posed* in the sense that it measures plastic deformation and that it can distinguish between path-dependent and path-independent behavior. We propose the following criteria that a well-posed strain rate should satisfy as:

A. It should possess a physical basis that relates it to some meaningful average of the average plastic strain rate in the plastic zone beneath the indenter.
B. It should be calculable for any loading path in which plastic deformation is taking place (e.g., CSR, CLH, CDR, CLR, LR, SRC…).
C. During elastic loading/unloading, the well-posed strain rate should be zero because there is no plastic deformation.
D. For a material in which the flow stress is path-independent, the measurement of hardness versus strain rate for self-similar indenters (cone, pyramid) along different loading paths should be identical.
E. For a material in which the flow stress is path-dependent, the measurement of hardness versus strain rate for self-similar indenters (cone, pyramid) along different loading paths in Fig. 1 should be different.

Below, we show that $\dot{\varepsilon}_A$ fails to satisfy D, at least for von Mises materials in simulations and polystyrene in experiments. The reader can confirm the trivial result that $\dot{\varepsilon}_A$ fails criterion C. We introduce a candidate definition for strain rate that meets criteria A and B, rigorously satisfies C, and satisfies D at least for the form of path-independent constitutive model we employ below. Whether or not this definition of strain rate can satisfy criterion E is largely an experimental issue, depending on how

strongly path-dependent the material is and how sensitive experimental capabilities are.

A New Definition of Strain Rate

In the Appendix, we derive an irreversible work-based definition of strain rate:

$$\dot{\varepsilon}_{\text{irr}} = \frac{\dot{h}}{h} - \frac{n}{n+1}\frac{H}{E_{\text{eff}}}\frac{\sqrt{A}}{h}\left(\frac{2\dot{P}}{P} - \frac{1}{2}\frac{\dot{A}}{A}\right) \tag{5}$$

where n $(1 \le n \le 2)$ is the power law exponent relating load to elastic depth during rebound,[41] and E_{eff} is the "effective" modulus defined in the Appendix, Eqs. 15 and 16, experimentally measured as the ratio of unloading stiffness (S) to the square root of projected contact area ($\sqrt{A}$). The physical significance of $\dot{\varepsilon}_{\text{irr}}$ is that $HAh\dot{\varepsilon}_{\text{irr}}$ is the rate of irreversible work carried out by indentation.

Equation 2 satisfies criteria A–C above. Its basis in irreversible thermodynamics satisfies A. $\dot{\varepsilon}_{\text{irr}}$ works along any loading path and therefore satisfies criterion B ($\dot{\varepsilon}_h$ does not). We show in the Appendix that $\dot{\varepsilon}_{\text{irr}} = 0$ for both elastic loading $(n = 2)$ and elastic unloading following plastic deformation $(1 \le n \le 2)$; thus, criterion C is satisfied (neither $\dot{\varepsilon}_h$ nor $\dot{\varepsilon}_A$ satisfy criterion C).

In the next section, we demonstrate that $\dot{\varepsilon}_{\text{irr}}$ satisfies criterion D, namely that hardness versus strain rate curves for path-independent materials generated from different loading paths coincide for a von Mises solid and polystyrene.

Analysis of Simulations and Experimental Data

The finite element analysis simulations have been described in previous publications.[42,43] These simulations employ the elastoplastic features of ABAQUS finite element code to model penetration of a conical indenter into a substrate. The indenter and solid are modeled as bodies of revolution. The indenter is a perfectly rigid cone with a half-angle $\alpha = 67.5$ degrees. The sample is modeled as a semi-infinite, elastic–plastic von Mises material, using quadrilateral axisymmetric 4 node isoparametric elements. In uniaxial loading, the material behaves according to:

$$\dot{\varepsilon} = \frac{\dot{\sigma}}{E_s} + \dot{\varepsilon}_p(\sigma, \varepsilon_p) \tag{6}$$

where $\dot{\varepsilon}$ is the total strain rate, $\dot{\varepsilon}_p$ is the plastic strain rate, σ the applied stress, and ε_p the plastic strain. Meshes were generated using GENMESH2D, and multi-point constraints (MPCs) were created using GENMPC2D. The mesh is further refined in regions near the edge of contact to minimize discrete displacement effects during creep or relaxation.

Indenter-specimen contact have been modeled as having a friction coefficient varying from 0.0 to 0.5.

To simulate a variety of material behaviors, we adopted a strain hardening creep law given by:

$$\dot{\bar{\varepsilon}} = \left(\kappa \bar{\sigma}^N [(M+1)\bar{\varepsilon}]^M\right)^{\frac{1}{1+M}} \tag{7}$$

where $\bar{\sigma}$, $\bar{\varepsilon}$, and $\dot{\bar{\varepsilon}}$ are von Mises equivalent stress, plastic strain, and plastic strain rate, respectively, N, M, and κ are material properties with $3.75 < N < 12$ and $0 > M > -0.52$ used for the simulations, and κ is varied to adjust the hardness/modulus ratio. This kind of constitutive law satisfies the definition of a path-independent material because strain rate is a unique function of (von Mises) stress and strain. Friction does not have an appreciable effect on the analysis other than to raise the hardness by a modest amount. The analysis provides a rationale for converting the strain rate sensitivity of the hardness, $m_H \equiv (\partial \ln H / \partial \ln \dot{\varepsilon}_A)_h$, to that of the flow stress, $m_\sigma \equiv \left(\partial \ln \bar{\sigma} / \partial \ln \dot{\bar{\varepsilon}}\right)_{\varepsilon}$, which for this model is $(1+M)/N$. In general, the two strain rate sensitivities are indistinguishable below about $H/E_r \approx 0.01$, and m_H is independent of the work-hardening exponent $\chi \equiv (\partial \ln \bar{\sigma} / \partial \ln \dot{\bar{\varepsilon}})_{\bar{\varepsilon}} = -M/N$.

Figures 4 and 5 show simulations in a material with high H/E_r. The limit in hardness is $(E_r \cot \alpha)/2 \approx 22.8$ GPa if the solid were fully elastic.[44] The material properties are $E_s = 100$ GPa, $\nu_s = 0.3$, $\kappa = 1.6 \times 10^8$ GPa^{-5} s$^{-0.8}$, $M = -0.2$, and $N = 5$. The indenter is infinitely stiff $(E_d \to \infty)$, and the coefficient of friction is zero. The simulations consist of 2-s-long constant displacement rate ramps followed by either constant load creep for 3 s or load relaxation for 2 s, followed by unloading.

Figure 5 shows the hardness–strain rate for the corresponding load–depth traces in Fig. 4. To compare between load relaxation and constant load

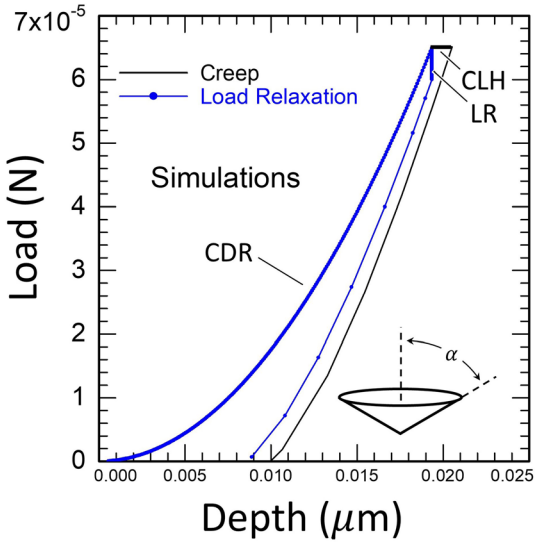

Fig. 4. Load–depth traces for simulated indents from Ref. 32 with constant displacement rate (*CDR*) loading segments followed by load relaxation (*LR*) or constant load creep (*CLH*).

creep, we employ $\dot{\varepsilon}_A$. Because $\dot{h}$ is constant and $\sqrt{A}$ is approximately proportional to h, $\dot{\varepsilon}_A$ slowly decreases during constant displacement rate loading. At the end of the loading segment, and as the simulation enters into either constant load hold or load relaxation, the strain rate jumps downward by a factor of about 8–10. This jump violates criterion D above, because, at the intersection where constant displacement rate loading transitions into constant load creep or load relaxation, the plastic strain rates for all three profiles should be the same. A discrete jump in the plastic strain rate at the intersection is not physical because plastic deformation is driven by stress (H), which is continuous across the intersection, and not, for instance, stress rate ($\dot{H}$), which is discontinuous. Lastly, load relaxation and constant load creep produce slightly different results when $\dot{\varepsilon}_A$ is used, which shows that $\dot{\varepsilon}_A$ violates criterion D.

The reason that $\dot{\varepsilon}_A$ does not match for constant displacement rate loading, load relaxation, and constant load creep in Fig. 5 is that $\dot{\varepsilon}_A$ is not a good measure of plastic deformation. During loading $\dot{\varepsilon}_A$ is approximately equal to $\dot{\varepsilon}_h$; and, therefore, by virtue of Eq. 26 in the Appendix, the product $H\dot{\varepsilon}_A$ is a good measure of the rate of *total* work being done on the system during loading. Yet, for such a high hardness/modulus ratio, the irreversible work only accounts for about 15–20% of the total work (see, for example, Ref. 45). During the constant load creep and load relaxation portions of the simulation, the product $H\dot{\varepsilon}_A$ more closely approximates the irreversible work done by the indenter. This is why the constant load creep and load relaxation data are so much closer to each other than they are to the constant displacement rate loading data.

Compiled hardness–strain rate data from simulations with a variety of material properties are shown in Figs. 6 and 7. In Fig. 6, the strain rate $\dot{\varepsilon}_A$ is used, while in Fig. 7, $\dot{\varepsilon}_{irr}$ is used. Each broken segment within a single family of curves corresponds to either the loading (black symbols) or constant load creep (other colors) portion of an individual finite element simulation. A straightforward transformation of the strain rate has allowed us to form master curves from different simulations sharing the same N, M but differing in κ and E_r. If two simulations are performed, corresponding to parameter values $(\kappa_1, E_{r,1})$ and $(\kappa_2, E_{r,2})$, then the curves from simulations 1 and 2 can be overlapped to form a master curve by shifting the strain rate scale in simulation 1 by:

$$\Delta \log \dot{\varepsilon}_A = -\frac{1}{1+M} \log \left[\left(\frac{\kappa_1}{\kappa_2} \right) \left(\frac{E_{r,1}}{E_{r,2}} \right)^N \right] \qquad (8)$$

Ideally, according to criterion D, the constant displacement rate loading and constant load creep segments should form continuous, overlapping master curves, but this is not the case when $\dot{\varepsilon}_A$ is used. In Fig. 6, the CDR and CLH master curves always differ from each other, and the differences increase with increasing H/E_{eff}. In Fig. 7, based on $\dot{\varepsilon}_{irr}$, the differences go away, so $\dot{\varepsilon}_{irr}$ meets criterion D for the path-independent materials governed by the flow law given by Eq. 7.

What about data from a real experiment? Polystyrene has a hardness/modulus ratio around 0.05, indicated by the shaded area in Figs. 6 and 7, so H-$\dot{\varepsilon}_A$ data should be measurably affected by the artifacts shown in Figs. 5 and 6. Figures 8 and 9 are re-analyses of the polystyrene data using $\dot{\varepsilon}_{irr}$ rather than $\dot{\varepsilon}_A$. The method for calculating area versus time, necessary for calculating instantaneous H and $\dot{\varepsilon}_A$, is described in the original reference.[21] Even though polystyrene is viscoelastic, it suffices to approximate E_{eff} as being constant, equal to 5.7 GPa measured in a 1-s unloading.[21] We observe that using $\dot{\varepsilon}_{irr}$ does not remove all of the (apparent) path dependence of polystyrene data shown in Figs. 2

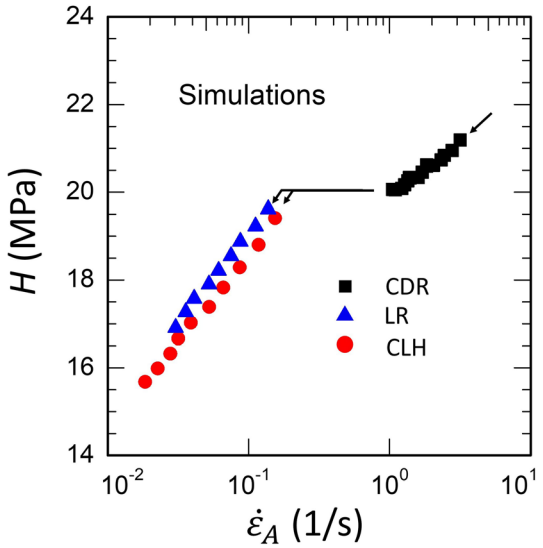

Fig. 5. Hardness (H)-strain rate data from Fig. 4 based on $\dot{\varepsilon}_A$ as the strain rate.

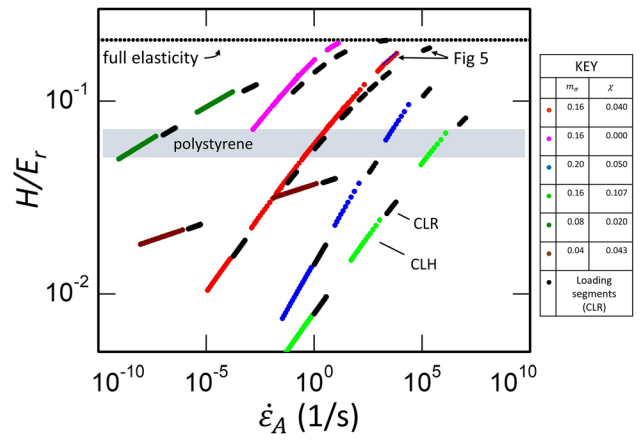

Fig. 6. Hardness–strain rate data for a range of material properties based on $\dot{\varepsilon}_A$ and plotted using the hardness to reduced modulus ratio (H/E_r) to group the data into families of curves.

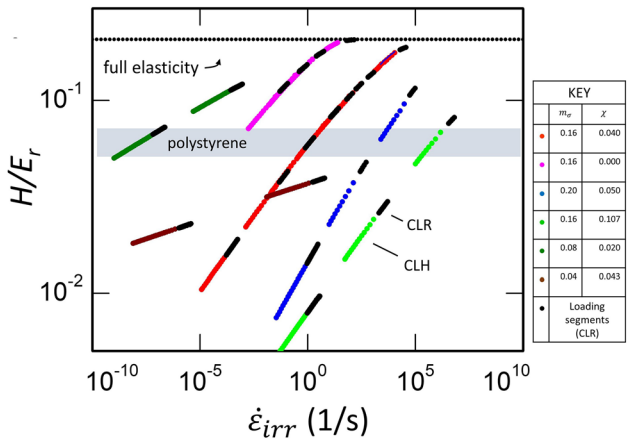

Fig. 7. Hardness–strain rate data for a range of material properties based on $\dot{\varepsilon}_{irr}$ and plotted using the hardness to reduced modulus ratio (H/E_r) to group the data into families of curves.

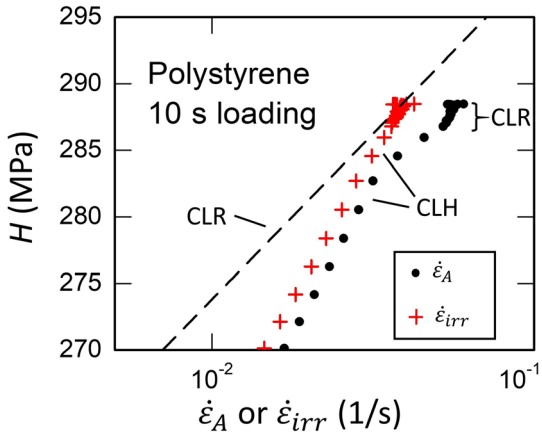

Fig. 8. Representation of polystyrene data from Ref. 11 comparing between $\dot{\varepsilon}_{irr}$ and $\dot{\varepsilon}_A$ for the 10-s loading data.

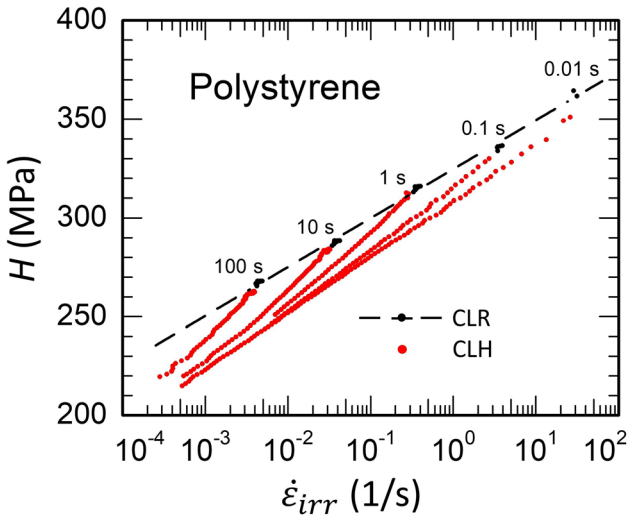

Fig. 9. Representation of polystyrene data comparing loading paths based on $\dot{\varepsilon}_{irr}$ for all loading rates.

and 3. Instead, $\dot{\varepsilon}_{irr}$ removes the misleading "transient" at the transition between the CLR and the constant load creep segments (Fig. 8). Apparently, this transient is caused by the same kind of (nonphysical) strain rate jump in $\dot{\varepsilon}_A$ that is present in the data simulations (Fig. 6) when transitioning from one loading path to another. (The hardness/modulus range for polystyrene is indicated by the shaded regions in Figs. 6 and 7). This transient is one reason why $\dot{\varepsilon}_A$ is not well-posed and $\dot{\varepsilon}_{irr}$ is.

In the case of polystyrene, we have not fully established why there are differences between hardness versus strain rate for constant load creep and CLR. Adiabatic heating at high strain rates is probably not the cause of the difference because the indents are too small even for the shortest timescales in the experiments, ~ 0.01 s, for adiabatic heating to be significant. Another explanation is that viscoelastic deformation violates path dependence and indirectly contributes to the measurements in a way that is not obvious. Based on several lines of evidence, however, we know that the CLR and constant load creep data in Figs. 8 and 9 are taken under conditions where viscoplastic deformation dominates and viscoelastic deformation has a relatively small effect.[21,45] Another possibility is that more free volume accumulates at high strain rates than at low strain rates, and its presence reduces the flow strength during subsequent constant load creep.

CONCLUSION

Complementary indentation tests (e.g., CLH, CSR, CDR, LR, CLR, RC in Fig. 1) can be used to probe path dependence in plastic deformation, thereby helping to reveal both the kinetics of deformation and the evolution of structure beneath the indenter. However, for this approach to work, the indentation strain should be *well-posed* in the sense that it meets criteria A–E. We have introduced $\dot{\varepsilon}_{irr}$, based on irreversible work, which meets criteria A–D. Criterion E, that is, being able to reveal path-dependent deformation when it is present, depends on how sensitive the experimental capabilities are. Because we were able to define $\dot{\varepsilon}_{irr}$ without having to make assumptions about the form of the flow law that governs plastic deformation, our approach is applicable to both pressure-independent (our simulations) and pressure-dependent (polystyrene) flow laws. In subtracting out the reversible work to obtain $\dot{\varepsilon}_{irr}$ we made the assumption that viscoelasticity is negligible, which might invalidate the analysis on highly viscoelastic materials (e.g., polymers). However, the analysis was shown to be effective in removing a (misleading) transient in polystyrene, a highly viscoelastic material.

The difference between $\dot{\varepsilon}_{\mathrm{irr}}$ and $\dot{\varepsilon}_{\mathrm{A}}$ can be substantial for high-hardness/modulus materials like ceramics and polymers, but is small for low-hardness/modulus materials like indium and other metals at high temperatures. Where this difference is important, it is largest during the loading segment in an indentation trace, so to compare data between different loading paths requires use of $\dot{\varepsilon}_{\mathrm{irr}}$. However, if one merely wishes to generate m_{H} data using, for instance, constant load creep, and one is not focused on exploring the path dependence of m_{H}, then $\dot{\varepsilon}_{\mathrm{A}}$ or $\dot{\varepsilon}_h$ should be suitable even for high-hardness/modulus materials.

ACKNOWLEDGEMENTS

This research (DSS) was funded by the United States National Science Foundation Directorate for Engineering (CMMI-1232731), United States Forest Service (18-JV-11111129-036) and Wisconsin Alumni Research Foundation (MSN215857). This research was supported in part by the U.S. Department of Agriculture, Forest Service.

CONFLICT OF INTEREST

On behalf of all authors, the corresponding author states that there is no conflict of interest.

APPENDIX: THEORY

We employ a heuristic argument based on irreversible work to arrive at an expression for the strain rate in an indentation experiment. The indenter is self-similar (cone or pyramid). Consider a nanoindentation experiment with h as the depth of penetration, measured between points on indenter and specimen that are far from the region of contact. h includes contributions from deformations in both the specimen and indenter. The indenter is linear elastic, while the specimen is both elastic and plastic. Let δh represent an increment of displacement during the time increment, δt. If P is the load, A the projected contact area, and $H = P/A$ the Meyer hardness, then the increment of total work done by the indenter is:

$$\delta W_{\mathrm{tot}} = P\delta h = HA\delta h \tag{9}$$

This work is directly related to the deformations taking place in the specimen and indenter, such that, for frictionless contact:

$$HA\delta h = \int_{\Sigma_s} \sigma_{ij}\delta\varepsilon_{ij}dV + \int_{\Sigma_d} \sigma_{ij}\delta\varepsilon_{ij}dV \tag{10}$$

where σ_{ij} and ε_{ij} are the tensor components of stress and strain, $\sigma_{ij}\delta\varepsilon_{ij}$ is work per unit volume, and the integral domains are specimen (Σ_s) and indenter (Σ_d). We now separate the specimen into Σ_{sp}, the region where plastic deformations dominate, and Σ_{se}, the region where elastic deformations dominate:

$$HA\delta h = \int_{\Sigma_{sp}} \sigma_{ij}\delta\varepsilon_{ij}dV + \int_{\Sigma_{se}} \sigma_{ij}\delta\varepsilon_{ij}dV + \int_{\Sigma_d} \sigma_{ij}\delta\varepsilon_{ij}dV \tag{11}$$

Up to this point, the treatment is exact given the assumptions stated. We now make some approximations. We approximate that, outside the plastic zone,[28,46] the plastic strain rate becomes vanishingly small and can be ignored. Likewise, inside the plastic zone, the elastic strain rate is negligible. We also approximate that the increment of reversible work embodied the second and third integrals in Eq. 11 can be calculated by evaluating the stored elastic energy that would be released if the experiment were interrupted at point i in Fig. 10, and then load was allowed to go to zero. For convenience, this point is shown located in the constant load part of the experiment, but it could also be located at anywhere along the load–depth trace. If the specimen is unloaded at this point, then the unloading curve takes the form of a power law provided by Oliver and Pharr:[41]

$$P = Kh_{\mathrm{e}}^{n} \tag{12}$$

where $h_{\mathrm{e}} = h - h_{\mathrm{f}}$ is the elastic depth shown in Fig. 10 and K a "constant" depending on the P and A at the beginning of unloading. The exponent, n, is a material parameter with $1 \le n \le 2$. The stored elastic energy is:

$$U_{\mathrm{el}} = \int_0^{h_e} K\xi^n \mathrm{d}\xi = \frac{1}{n+1}Ph_{\mathrm{e}} \tag{13}$$

It is awkward to base our analysis on h_{e}, so we transform from $U_{\mathrm{el}} = U_{\mathrm{el}}(P, h_{\mathrm{e}})$ to $U_{\mathrm{el}} = U_{\mathrm{el}}(P, A)$. The instantaneous contact stiffness is given by:

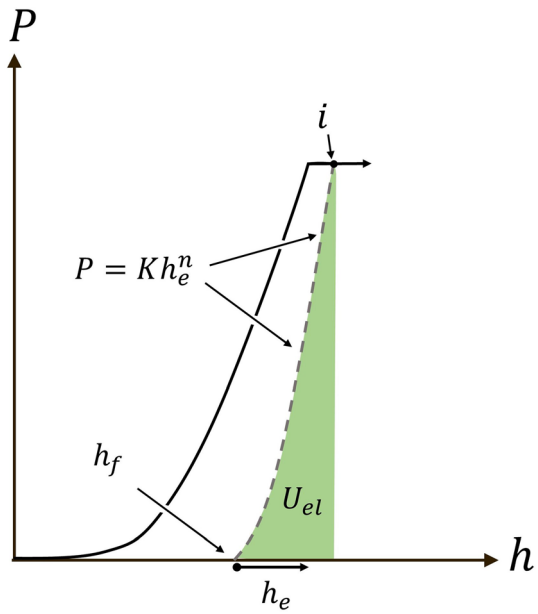

Fig. 10. Load–depth (P–h) trace showing interrupted creep experiment in which the specimen is unloaded at the point i rather than being allowed to continue. The stored elastic energy at point i is U_{el}.

$$S = \left.\frac{\partial P}{\partial h}\right|_{\text{unloading}} = nKh_e^{n-1} = \frac{nP}{h_e} \tag{14}$$

The instantaneous contact stiffness is also:[41]

$$S = E_{\text{eff}}\sqrt{A} \tag{15}$$

With:

$$\frac{1}{E_{\text{eff}}} = \frac{1}{\beta E_r} = \frac{1}{\beta}\left[\frac{1-\nu_d^2}{E_d} + \frac{1-\nu_s^2}{E_s}\right] \tag{16}$$

where E and ν are Young's modulus and Poisson's ratio, respectively, and the subscripts d and s refer to the indenter and the specimen, respectively. E_{eff} is measured directly in a nanoindentation experiment, while β is a numerical factor which allows the experimenter to estimate E_r, the reduced modulus from contact problems. Solving Eqs. 14 and 15 for h_e in terms of P and A, we may substitute into Eq. 13 to obtain stored elastic energy as:

$$U_{\text{el}} = \frac{n}{n+1}\frac{P^2}{E_{\text{eff}}\sqrt{A}} \tag{17}$$

An increment in stored (recoverable) elastic energy, δU_{el}, can be substituted for the 2nd and 3rd integrals in Eq. 11 to obtain:

$$HA\delta h = \int_{\Sigma_{sp}} \sigma_{ij}\delta\varepsilon_{ij}dV + \delta\left[\frac{n}{n+1}\frac{P^2}{E_{\text{eff}}\sqrt{A}}\right] \tag{18}$$

Generally, both P and A evolve during an experiment, so that the expression in square brackets can be expanded:

$$HA\delta h = \int_{\Sigma_{sp}} \sigma_{ij}\delta\varepsilon_{ij}dV + \frac{n}{n+1}\frac{P^2}{E_{\text{eff}}\sqrt{A}}\left(\frac{2\delta P}{P} - \frac{\delta\sqrt{A}}{\sqrt{A}}\right) \tag{19}$$

We now isolate the portion on the right-hand side that represents an increment of irreversible work:

$$HA\delta h - \frac{n}{n+1}\frac{P^2}{E_{\text{eff}}\sqrt{A}}\left(\frac{2\delta P}{P} - \frac{1}{2}\frac{\delta A}{A}\right) = \int_{\Sigma_{sp}} \sigma_{ij}\delta\varepsilon_{ij}dV \equiv \delta W_{\text{irr}} \tag{20}$$

where we have also used $\delta\sqrt{A}/\sqrt{A} = (1/2)(\delta A/A)$. We introduce the volume of the plastic zone as:

$$\Omega_p = \int_{\Sigma_{sp}} \mathrm{d}V \tag{21}$$

and designate σ_Y as the yield stress measured under uniaxial loading. Dividing both sides of Eq. 20 by $\sigma_Y\Omega_p$ and factoring out h on the left-hand side, we have:

$$\frac{H}{\sigma_Y}\frac{Ah}{\Omega_p}\left[\frac{\delta h}{h} - \frac{n}{n+1}\frac{H}{E_{\text{eff}}}\frac{\sqrt{A}}{h}\left(\frac{2\delta P}{P} - \frac{1}{2}\frac{\delta A}{A}\right)\right] = \frac{1}{\sigma_Y\Omega_p}\int_{\Sigma_{sp}} \sigma_{ij}\delta\varepsilon_{ij}\mathrm{d}V \tag{22}$$

Next, we divide through by the increment of time, δt, and employ $\delta h/\delta t \to \dot{h}$, etc., so that the right-hand side of the equation represents an average, "characteristic" plastic strain rate in the plastic zone, $\langle\dot{\varepsilon}_p\rangle$:

$$\frac{H}{\sigma_Y}\frac{Ah}{\Omega_p}\left[\frac{\dot{h}}{h} - \frac{n}{n+1}\frac{H}{E_{\text{eff}}}\frac{\sqrt{A}}{h}\left(\frac{2\dot{P}}{P} - \frac{1}{2}\frac{\dot{A}}{A}\right)\right] = \frac{1}{\sigma_Y\Omega_p}\int_{\Sigma_{sp}} \sigma_{ij}\dot{\varepsilon}_{ij}dV \equiv \langle\dot{\varepsilon}_p\rangle \tag{23}$$

The numerical factor H/σ_Y on the left-hand side of Eq. 23 is the familiar constraint factor relating hardness to yield strength, whereas Ah/Ω_p is the ratio of indent volume to plastic zone volume. Both of these ratios have been studied extensively in the literature.[2,38,46] The expression inside the square brackets in Eq. 23 is evidently a kind of strain rate that excludes the reversible deformations responsible for elastic rebound. We therefore propose a new definition of strain rate for an indentation test in which arbitrary combinations of h, P, and A might vary as functions of time as:

$$\dot{\varepsilon}_{\text{irr}} = \frac{\dot{h}}{h} - \frac{n}{n+1}\frac{H}{E_{\text{eff}}}\frac{\sqrt{A}}{h}\left(\frac{2\dot{P}}{P} - \frac{1}{2}\frac{\dot{A}}{A}\right) \tag{24}$$

In more conventional terminology using $\beta = 2/\sqrt{\pi}$:

$$\dot{\varepsilon}_{\text{irr}} = \frac{\dot{h}}{h} - \frac{n}{n+1}\frac{\sqrt{\pi}}{2}\frac{H}{E_r}\frac{\sqrt{A}}{h}\left(\frac{2\dot{P}}{P} - \frac{1}{2}\frac{\dot{A}}{A}\right) \tag{25}$$

Note that we have not made any assumptions about the relationships that govern plastic flow inside the integral on the right-hand side of Eq. 23. As a consequence, Eqs. 23–25 should be equally valid for both pressure-independent and pressure-dependent yielding. Also, the analysis does not depend on the precise values of Ω_p and σ_Y, nor whether, for instance, σ_Y is measured in compression or tension or represents the initial yield stress or yield stress after some other level of strain.

Following from Eq. 9, the rate of total work being done by the indenter is:

$$\dot{W}_{\text{tot}} = hAH\dot{\varepsilon}_h = hAH\frac{\dot{h}}{h} \tag{26}$$

For load relaxation, the indenter does no work, so $\dot{W}_{\text{tot}} = 0$. Instead, plastic deformation is driven entirely by stored elastic energy in the indenter and specimen. The rate of irreversible work for all loading profiles is:

$$\dot{W}_{\text{irr}} = hAH\dot{\varepsilon}_{\text{irr}} = hAH\left[\frac{\dot{h}}{h} - \frac{n}{n+1}\frac{H}{E_{\text{eff}}}\frac{\sqrt{A}}{h}\left(\frac{2\dot{P}}{P} - \frac{1}{2}\frac{\dot{A}}{A}\right)\right] \quad (27)$$

which gives a non-zero value even for load relaxation, as long as plastic deformation is taking place. The rate of reversible work is:

$$\dot{W}_{\text{rev}} = hAH(\dot{\varepsilon}_{\text{h}} - \dot{\varepsilon}_{\text{irr}}) = hAH\left[\frac{n}{n+1}\frac{H}{E_{\text{eff}}}\frac{\sqrt{A}}{h}\left(\frac{2\dot{P}}{P} - \frac{1}{2}\frac{\dot{A}}{A}\right)\right] \quad (28)$$

Lastly, criterion C requires that $\dot{\varepsilon}_{\text{irr}}$ be zero for (1) purely elastic loading and (2) unloading or reloading following elastic–plastic indentation. Our definition of $\dot{\varepsilon}_{\text{irr}}$ satisfies both instances Firstly, according to Sneddon,[44] loading an ideally elastic solid by a cone with cone half-angle, α, gives $\sqrt{A}/h = (2/\sqrt{\pi})\tan\alpha$, $H/E_{\text{r}} = \cot\alpha/2$, and $n = 2$ ($\alpha = 70.3°$ for a cone with same area–depth profile as a Berkovitch indenter). Also, $\dot{P}/P = \dot{A}/A = 2\dot{h}/h$. Substituting these values into Eq. 25 reveals $\dot{\varepsilon}_{\text{irr}} = 0$. Secondly, for elastic unloading or reloading after an (elastic–plastic) indent, such as shown in Fig. 10, $1 \le n \le 2$ and $dh = dh_{\text{e}}$. Under these conditions, $\dot{A}/A = 2(n-1)\left(\dot{h}/h_{\text{e}}\right)$ and $\dot{P}/P = n\left(\dot{h}/h_{\text{e}}\right)$. Substitution into Eq. 25 again reveals $\dot{\varepsilon}_{\text{irr}} = 0$.

REFERENCES

1. T.O. Mulhearn and D. Tabor, *J. Inst. Met.* 89, 7 (1960).
2. D. Tabor, *Rev. Phys. Techn.* 1, 145 (1970).
3. A. Rar, S. Sohn, W. C. Oliver, D. L. Goldsby, T. E. Tullis, and G. M. Pharr, in MRS Fall Meeting, Vol. 841 (Materials Research Society, Warrendale, PA 15086, United States, Boston, MA, United States, 2005), pp. 119–124.
4. M.J. Mayo and W.D. Nix, *Acta Metall.* 36, 2183 (1988).
5. D.S. Stone and K.B. Yoder, *J. Mater. Res.* 9, 2524 (1994).
6. K.B. Yoder, A.A. Elmustafa, J.C. Lin, R.A. Hoffman, and D.S. Stone, *J. Phys. D Appl. Phys.* 36, 884 (2003).
7. K. Durst and V. Maier, *Curr. Opin. Solid State Mater. Sci.* 19, 340 (2015).
8. V. Maier-Kiener and K. Durst, *JOM* 69, 2246 (2017).
9. S.P. Hannula, D.S. Stone, and C.Y. Li, *J. Met.* 36, 53 (1984).
10. K.K. Alaneme, M.O. Bodunrin, and E.A. Okotete, *J. King Saud Univ. Engr. Sci.* 35, 62 (2023).
11. A.P. Carvalho and R.B. Figueiredo, *J. Mater. Sci.* 58, 8130 (2023).
12. H.N. Fowler, A. Loaiza, D.F. Bahr, J.E. Blendell, and C.A. Handwerker, *J. Electron. Mater.* 52, 7365 (2023).
13. F. Khodabakhshi, M.H. Farshidianfar, A.P. Gerlich, A. Khajepour, V. Nagy Trembošová, M. Mohammadi, S.I. Shakil, and M. Haghshenas, *Mater. Sci. Eng. A* 862, 144437 (2023).
14. X. Niu, G. Dong, X. Li, X. Geng, and J. Zhou, *Microelectron. Reliab.* 128, 114429 (2022).
15. L. Yang, Y. Chen, J. Miller, W.J. Weber, H. Bei, and Y. Zhang, *Mater. Sci. Eng. A* 856, 143685 (2022).
16. L.W. Yang, C.Y. Wang, M.A. Monclús, L. Lu, J.M. Molina-Aldareguía, and J. Llorca, *Scr. Mater.* 154, 54 (2018).
17. J. Cao, K. Wang, W. Ma, J. Ren, H. Nie, W. Dang, X. Liang, T. Yao, and X. Zhao, *Int. J. Pressure Vessels Piping* 199, 104776 (2022).
18. L. Lv, H. Lin, and T. Jin, *Vacuum* 185, 110026 (2021).
19. D. Wu, X. Huang, X. Duan, Y. Jiang, D. Shi, L. Chang, L. Zhang, and J. He, *J. Phys. Chem. C* 127, 4749 (2023).
20. L.H. He and M.V. Swain, *J. Mech. Behav. Biomed. Mater.* 1, 18 (2008).
21. J.E. Jakes, R.S. Lakes, and D.S. Stone, *J. Mater. Res.* 27, 475 (2012).
22. J. Chen, B.D. Beake, G.A. Bell, Y. Tait, and F. Gao, *J. Exp. Nanosci.* 11, 695 (2016).
23. M.L. Oyen, *Acta Mater.* 55, 3633 (2007).
24. C.A. Schuh, A.C. Lund, and T.G.G. Nieh, *Acta Mater.* 52, 5879 (2004).
25. S.N.G. Chu and J.C.M. Li, *J. Mater. Sci.* 12, 2200 (1977).
26. D.L. Goldsby, A. Rar, G.M. Pharr, and T.E. Tullis, *J. Mater. Res.* 19, 357 (2004).
27. J. Lu, S. Suresh, and G. Ravichandran, *J. Mech. Phys. Solids* 51, 1923 (2003).
28. C. Zener and J.H. Hollomon, *J. Appl. Phys.* 17, 69 (1946).
29. E.W. Hart and H.D. Solomon, *Acta Metall.* 21, 295 (1973).
30. T.L. Briggs and J.D. Campbell, *Acta Metall.* 20, 711 (1972).
31. H. Conrad, in *High-Strength Materials* , edited by V. F. Zackay (Berkeley, 1964), p. 436.
32. G. Taylor, *Prog. Mater. Sci.* 36, 29 (1992).
33. A.A. Elmustafa and D.S. Stone, *Mater. Lett.* 57, 1072 (2003).
34. B.N. Lucas and W.C. Oliver, *Metall. Mater. Trans. A* 30A, 601 (1999).
35. P.S. Phani, W.C. Oliver, and G.M. Pharr, *J. Mech. Phys. Solids* 154, 104527 (2021).
36. S. P. Hannula, D. Stone, and C. Y. Li, in Materials Research Society, Electronic Packaging Materials Science Symposia, Vol. 40 (1985), p. 218.
37. V. Maier, K. Durst, J. Mueller, B. Backes, H.W. Höppel, and M. Göken, *J. Mater. Res.* 26, 1421 (2011).
38. K.L. Johnson, *J. Mech. Phys. Solids* 18, 115 (1970).
39. M.F. Doerner and W.D. Nix, *J. Mater. Res.* 1, 601 (1986).
40. J.E. Jakes, R.S. Lakes, and D.S. Stone, *J. Mater. Res.* 27, 463 (2012).
41. W.C. Oliver and G.M. Pharr, *J. Mater. Res.* 7, 1564 (1992).
42. A.A. Elmustafa, S. Kose, and D.S. Stone, *J. Mater. Res.* 22, 926 (2007).
43. A.A. Elmustafa and D.S. Stone, *J. Mater. Res.* 22, 2912 (2007).
44. I.N. Sneddon, *Int. J. Eng. Sci.* 3, 47 (1965).
45. Y.-T. Cheng and C.-M. Cheng, *Mater. Sci. Eng. R* 44, 91 (2004).
46. S.S. Chiang, D.B. Marshall, and A.G. Evans, *J. Appl. Phys.* 53, 298 (1982).